Nanoscale Res Lett (2010) 5:1437–1441
DOI 10.1007/s11671-010-9658-2

NANO EXPRESS

Fabrication of Porous TiO_2 Hollow Spheres and Their Application in Gas Sensing

Gang Yang · Peng Hu · Yuebin Cao · Fangli Yuan · Ruifen Xu

Received: 31 March 2010 / Accepted: 19 May 2010 / Published online: 3 June 2010

Abstract In this work, porous TiO_2 hollow spheres with an average diameter of 100 nm and shell thickness of 20 nm were synthesized by a facile hydrothermal method with NH_4HCO_3 as the structure-directing agent, and the formation mechanism for this porous hollow structure was proved to be the Ostwald ripening process by tracking the morphology of the products at different reaction stages. The product was characterized by SEM, TEM, XRD and BET analyses, and the results show that the as-synthesized products are anatase phase with a high surface area up to 132.5 m^2/g. Gas-sensing investigation reveals that the product possesses sensitive response to methanal gas at 200°C due to its high surface area.

Keywords Porous TiO_2 · Hollow sphere · Hydrothermal synthesis · Gas sensing

Introduction

In recent decades, nanostructured materials have attracted much attention due to their special structure and excellent properties in optics, electrics, magnetics, chemistry, etc. [1–4]. In particular, titanium dioxide (TiO_2), as an important IV–VI group semiconductor with a band gap of 3.2 eV, has been widely applied in chemical industry, electronic industry, environmental protection, cosmetics industry, medical science and so on [3–6]. In order to improve their performances, nanostructured TiO_2 with various structures, including nanoparticles [7], nanotubes [8], nanorods [9] and nanospheres [10], has been investigated and fabricated successfully. Among these structures, hollow structure, as a new special class of materials, has increasingly attracted interest because of its higher specific surface area, lower density, greater delivering ability, better permeation and stronger light-harvesting capacity compared to solid ones [11–13].

Up to now, many synthetic strategies have been devoted to synthesize nanomaterials with hollow structures. Among them, hard-template is typically used to fabricate hollow spheres and many different materials, such as carbon (C), polystyrene (PS), styrene-methyl methacrylate copolymer (PSMMA), have been used as templates [14–17]. These preparations often require removal of the templates after synthesis, which may damage the desired configurations of the hollow spheres. Other methods, including sol–gel, microemulsion and self-assembly method [18–20], are also adopted to synthesize hollow structures. However, these methods always need to add surfactant or organic solvent, which perhaps introduces impurities to the products and increase the cost.

In this paper, we report a facile method to fabricate porous TiO_2 spheres with hollow structure, and this work is based on our previous work to synthesize monodisperse Fe_3O_4 hollow microspheres [21]. Based on the initial reports, it should be noted that NH_4HCO_3 plays an important role in the formation of the hollow structure and can be further confirmed in the current report. The synthesized products are composed of porous shell, which makes the sample a large specific surface area of 132.5 m^2/g. Gas-sensing investigation reveals that the product possesses

G. Yang · R. Xu
College of Materials Science and Engineering, Beijing University of Chemical Technology, 100029 Beijing, China

G. Yang · P. Hu · Y. Cao · F. Yuan (✉)
State Key Laboratory of Multi-phase Complex System, Institute of Process Engineering, Chinese Academy of Sciences, 100190 Beijing, China
e-mail: flyuan@home.ipe.ac.cn

sensitive response to methanal gas due to its high surface area, and the results reveal that this special structure may have potential properties and applications in some related fields.

Experimental

Preparation of TiO_2 Hollow Spheres

All reagents are analytically pure and used without further purification. In a typical experiment, a mixture of 4 mL of tetrabutyl titanate (TBOT) and 20 mL of ethanol was dropped into 100 mL of deionized water under magnetic stirring to form an ivory-white sol. Then, the resulting mixture was divided into three parts, and one of them was transferred to a 100-mL Teflon-lined autoclave, followed by the addition of 1 g of NH_4HCO_3 and filling with ethanol up to 70% of the total volume. The autoclave was maintained at 180°C for 48 h. After reaction, the autoclave was cooled to room temperature. The product was obtained by centrifuging and sequentially washing with water and ethanol for several times and then dried in a vacuum oven at 60°C for 5 h.

Characterization

The phase of the product was determined by X-ray diffraction (XRD) patterns, which were recorded with a Philips X'Pert PRO MPD X-ray diffractometer using Cu Kα radiation ($\lambda = 1.54178$ Å). The morphology and structure of the product were then observed by a scanning electron microscope (SEM, JEOL JSM-6700F) and a transmission electron microscope (TEM, JEOL JEM-2100). The pore size distribution and Brunauer–Emmett–Teller (BET) surface area were calculated from the nitrogen adsorption–desorption isotherm that is obtained by using an Autosorb-1 automatic surface area and pore size distribution analyzer. The gas-sensing property was tested in a home-made instrument as reported earlier [22].

Results and Discussion

The morphology and structure of the synthesized products are shown in Fig. 1. From the typical SEM image of the obtained products shown in Fig. 1a, we can see that uniformly spherical particles with a diameter of 100 nm were obtained in the experiment, and no particles with other shape were found. A magnified SEM image reveals the detailed morphology, as shown in the inset of Fig. 1a, which indicates that as-synthesized spheres were composed of fine nanocrystallites, with a rough surface and maybe have pores in it. The porous hollow structure was further investigated by the TEM image as shown in Fig. 1b, and the intensive contrast between center and edge of the spheres indicates the formation of hollow structure in the final products, and the shell thickness of the spheres is about 20–25 nm. The bright spots scattered in the dark shell also confirm that the shell is porous. The crystal

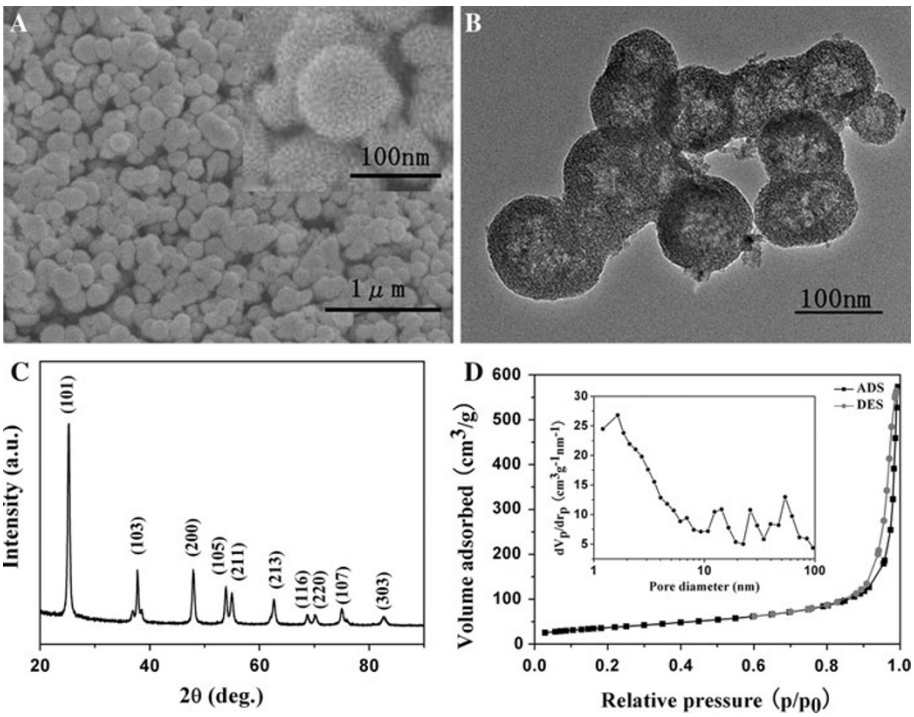

Fig. 1 **a** SEM image, **b** TEM image, **c** XRD patterns, **d** Nitrogen absorption–desorption isotherms and corresponding pore size distribution of TiO_2 hollow spheres synthesized at 180°C for 48 h

structure of the TiO_2 sample was determined by XRD analysis as shown in Fig. 1c. All the diffraction peaks can be well indexed to anatase phase of TiO_2 (JCPDS 71-1169). No peaks of impurities were detected in the XRD patterns, indicating the high purity of the products. The strong and sharp peaks also confirm the well crystallization of the synthesized products.

Figure 1d gives the nitrogen adsorption–desorption isotherms and corresponding pore size distribution of the TiO_2 product. The isotherm shown in the Fig. 1d can be well classified as type IV isotherm, indicating the formation of a typical porous structure [23]. The corresponding pore size distribution (the inset in Fig. 1d) was calculated by means of Barret–Joyner–Halenda (BJH) method. From the distribution curve, we can see that porous TiO_2 hollow spheres possess a broad pore size distribution due to the coexistence of mesoporous and micropores, but the pores with diameter of $1 \sim 3$ nm are dominant in the final products. The BET analysis confirms the high specific surface area (132.5 m^2/g) of the product, which comes from the formation of the porous hollow structures.

In order to explore the evolution process of the porous hollow structure, time-dependant experiments were conducted, and Fig. 2 gives the TEM images of products obtained at different reaction times. At the beginning of the hydrothermal reaction, titanium dioxide crystallized gradually and formed lots of small nanocrystallites. At the same time, NH_4HCO_3 was decomposed to NH_3 and CO_2 at heating condition. These gas bubbles and TiO_2 nanoparticles tend to aggregate together to minimize the interfacial energy, and the spherical aggregates are then formed by aggregation of original nanocrystallites nucleated on the gas–liquid interface as shown in Fig. 2a. The solid aggregates then followed by a solid core evacuation and a hollowing effect are observed for those with a longer reaction time of 24 h (Fig. 2b), which is due to the continuous outward growth of the fine nanocrystallites and the gas bubbles gathered in the center of spheres [24]. As the reaction time further increased, the migration sustainedly carried out to a certain degree, and the hollow sphere structure was obviously obtained (Fig. 2c). Based on the experimental results and analysis, the formation mechanism of hollow structure can be interpreted as the Ostwald ripening process [21]. After the formation of the hollow spheres, lots of gas bubbles still existed in the shell, and they acted as templates for the formation of the loose packed shell. Thus, the hollow TiO_2 spheres with a porous shell were finally obtained. XRD analyses reveal the different crystalline phases of products obtained at different reaction times, typically are amorphism, brookite and anatase. Accordingly, porous TiO_2 spheres with different phases could be well controlled by adjusting the reaction time in our experiments.

To investigate the adsorption property of synthesized products, 0.1 g of sample was added into 100 mL of aqueous methylene blue (MB) solution with different concentrations, and then the mixture was placed in the darkroom under magnetic stirring for 10 s. The adsorption property of the product for MB was measured by the MB concentration change before and after adsorption. The concentration of MB was detected using an UV–vis spectrophotometer. The color change of the MB solution (100 mg/L) after adsorption was shown in Fig. 3. The color contrast of the MB solution before and after adsorption indicates the excellent adsorption ability of the porous TiO_2 hollow spheres for organic dyestuff. The test results of adsorption property of the sample to MB were shown in Table 1. The adsorption rate and adsorption quantity are calculated by the Eqs. 1 and 2, respectively.

$$\mu = (c_0 - c)/c_0 = (A_0 - A)/A_0 \quad (1)$$

$$q = (c_0 - c) \cdot V/m \quad (2)$$

(Here, μ is the adsorption rate; q is the adsorption quantity; c_0 and c are MB concentrations before and after mixing, respectively; A_0 and A are absorbencies of the MB solution before and after mixing, respectively; V is the volume of the solution, and m is the mass of TiO_2 sample.)

From the Table 1, it can be seen that $96 \sim 98\%$ of MB in the solution can be adsorbed by the TiO_2 sample at a low MB concentration of 50 and100 mg/L. When the concentration of MB increases to 200 mg/L, the adsorption quantity of the sample is up to 170.9 mg/g. The adsorption quantity has no obvious increase when the concentration of

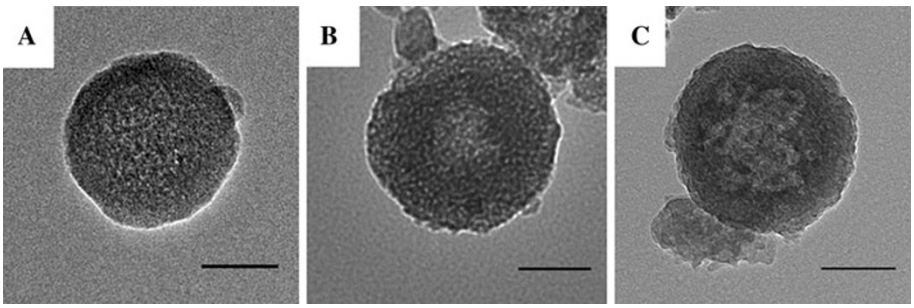

Fig. 2 TEM images of products obtained at different reaction times: **a** 0 h, **b** 24 h and **c** 48 h. *Scale bar* 50 nm

Fig. 3 The color contrast of 100 mg/L MB solution before and after adsorption. The *left* shows the primary solution, and the *right* is the solution after adsorption by the porous TiO_2 sample for 10 s

Table 1 The adsorption property test results of the TiO_2 hollow sphere product

MB concentration (mg/L)	Adsorption rate (%)	Adsorption quantity (mg/g)
50	96.49	48.25
100	97.78	97.78
200	85.45	170.9
400	42.96	171.8

MB further increases (400 mg/L), which indicates the saturated adsorption quantity of the sample is about 171 mg/g. The high adsorption ability of this product indicates that the porous TiO_2 hollow spheres may be used as adsorbent in some fields such as wastewater treatment.

As the synthesized TiO_2 hollow sphere powder has a high specific surface area and intense adsorption ability, it is natural to consider its application in specific gas detection. The gas sensor was assembled using thin film prepared from the porous TiO_2 hollow sphere powder. Figure 4a–c gives the typical isothermal response curves of the thin film sensor exposed to methanal (HCHO) gas at different operating temperatures (200, 300 and 400°C). In the gas-sensing test, HCHO gas was diluted in water vapor, and the flow velocity of the mixed gas was controlled at 0.6 L/min. The sensor sensitivity was defined as the slope of the R_a/R_g versus c curve, and herein, R_a is the resistance value of the sensor in clean air, R_g is the resistance value of the sensor in specific gas under test and c is the HCHO gas concentration.

Based on the isothermal response curves, it can be concluded that the resistance value of the sensor decreases sharply when the HCHO gas passes the sensor, which indicated the good response speed of fabricated gas sensor. As time increases, gas diffusion slows down in the film, leading to a corresponding slowdown of the resistance decrease rate, resistivity finally reaching stability. When the analyte is removed, the resistance value rises immediately and restores fast. In general, it is believed that the sensing mechanism includes two reactions [25, 26]. First, oxygen adsorbed on the TiO_2 sample surface captures electrons from TiO_2 and transforms into O_{ad}^-. Then, in the reductive gas condition (here is methanal), O_{ad}^- will be

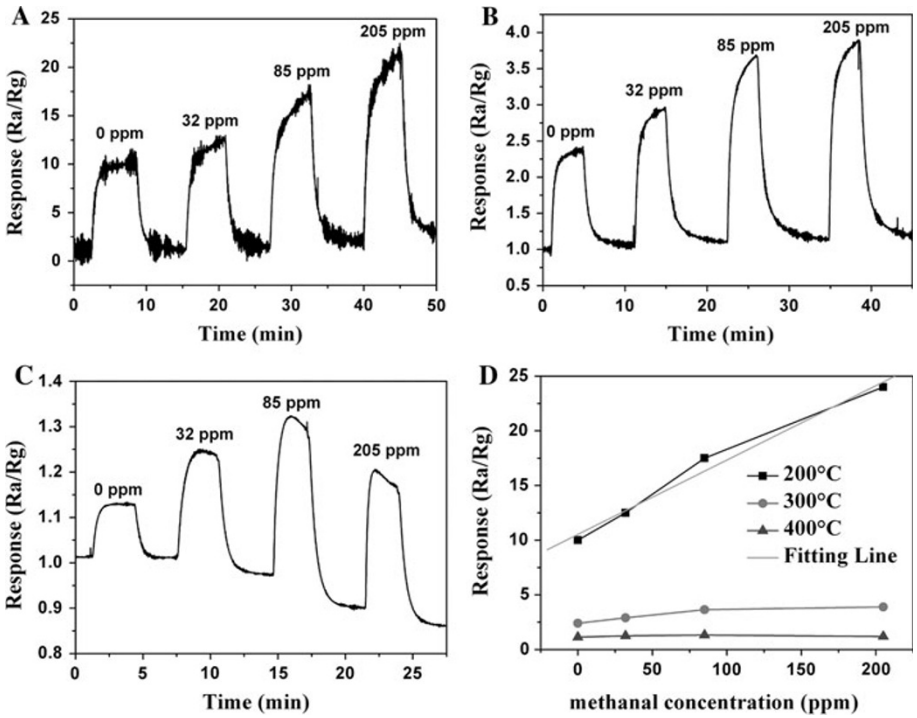

Fig. 4 Response curves to HCHO at **a** 200°C, **b** 300°C, **c** 400°C and **d** the response magnitude, R_a/R_g versus HCHO gas concentration

reduced and its electron is given back to TiO_2, leading the electron density to increase. Therefore, in macro-view, when the thin film sensor is exposed to HCHO, the resistance value will decrease, and the relative change of the values at different gas concentrations is used to characterize gas sensitivity. Figure 4d shows the curve of sensor-normalized resistivity (R_a/R_g) versus HCHO gas concentration at different operating temperatures. It can be clearly seen that the gas sensor at operating temperature of 200°C presents a much higher gas-sensing property than the ones operated at 300 and 400°C. In addition, the sensor shows a relatively linear dependence on the HCHO concentration at 200°C, and the fitting line equation with the correlation coefficient of 0.9914 is as follows:

$$R_a/R_g = 10.52767 + 0.06798C_{HCHO} \quad (3)$$

Up to now, few papers about TiO_2 hollow spheres applied in gas sensing are reported. Moreover, the nanoscale TiO_2 materials with other morphologies do not exhibit very good gas sensitivity, and the operating process needs to be conducted in a higher temperature condition [27–29]. Compared to previous reported TiO_2 samples, our porous TiO_2 hollow spheres have a good performance in gas sensing at lower operating temperature. This satisfactory gas sensitivity attributed to the porous structure and large specific surface area indicates the importance of the microstructure control of gas-sensing layers.

Conclusions

In summary, porous TiO_2 hollow spheres with anatase phase were prepared by a hydrothermal method, and SEM and TEM investigation reveals that the products have a uniform diameter and shell thickness of about 100 nm and 20–25 nm, respectively. This preparation process is more facile compared to other methods reported. The formation mechanism of the porous hollow structure can be attributed to the Ostwald ripening. The results also confirmed that the as-synthesized hollow spheres exhibit high adsorption ability for organic dyestuff and excellent gas sensitivity to HCHO of the TiO_2 thin firm sensor performed at relatively low operating temperature (200°C).

Acknowledgments The authors acknowledge the financial support from the National Nature Science Foundation of China (No. 10905068 and 50974111).

References

1. S.J. Pearton, D.P. Norton, K. Ip, Y.W. Heo, T. Steiner, Superlattices Microstruct. **34**, 3 (2003)
2. Y.N. Xia, P.D. Yang, Y.G. Sun, Y.Y. Wu, B. Mayers, B. Gates, Y.D. Yin, F. Kim, H.Q. Yan, Adv. Mater. **15**, 353 (2003)
3. M. Ni, M.K.H. Leung, D.Y.C. Leung, K. Sumathy, Renew. Sust. Energ. Rev. **11**, 401 (2007)
4. X.B. Chen, S.S. Mao, Chem. Rev. **107**, 2891 (2007)
5. E. Stathatos, Y.J. Chen, D.D. Dionysiou, Sol. Energy Mater. Sol. Cells **92**, 1358 (2008)
6. M.G. Manera, P.D. Cozzoli, M.L. Curri, G. Leo, R. Rella, A. Agostiano, L. Vasanelli, Synth. Met. **148**, 25 (2005)
7. K.S. Yoo, T.G. Lee, J. Kim, Microporous Mesoporous Mater. **84**, 211 (2005)
8. Y.Y. Song, F.S. Stein, S. Bauer, P. Schmuki, J. Amer. Chem. Soc. **131**, 4230 (2009)
9. Q.S. Wei, K. Hirota, K. Tajima, K. Hashimoto, Chem. Mater. **18**, 5080 (2006)
10. L. Yang, Y. Lin, J.G. Jia, X.P. Li, X.R. Xiao, X.W. Zhou, Microporous Mesoporous Mater. **112**, 45 (2008)
11. L. Jiang, Y.J. Zhong, G.C. Li, Mater. Res. Bull. **44**, 999 (2009)
12. D.G. Shchukin, R.A. Caruso, Chem. Mater. **16**, 2287 (2004)
13. Y.X. Zhang, G.H. Li, Y.C. Wu, Y.Y. Luo, L.D. Zhang, J. Phys. Chem. B **109**, 5478 (2005)
14. C.Y. Song, W.J. Yu, B. Zhao, H.L. Zhang, C.J. Tang, K.Q. Sun, X.C. Wu, L. Dong, Y. Chen, Catal. Commun. **10**, 650 (2009)
15. X. Du, J.H. He, Mater. Res. Bull. **44**, 1238 (2009)
16. J.P. Wang, Y. Bai, M.Y. Wu, J. Yin, W.F. Zhang, J. Power Sources **191**, 614 (2009)
17. R.B. Zheng, X.W. Meng, F.Q. Tang, Appl. Surf. Sci. **255**, 5989 (2009)
18. Y.X. Hu, J.P. Ge, Y.G. Sun, T.R. Zhang, Y.D. Yin, Nano Lett. **7**, 1832 (2007)
19. G.L. Li, E.T. Kang, K.G. Neoh, X.L. Yang, Langmuir **25**, 4361 (2009)
20. T.Z. Ren, Z.Y. Yuan, B.L. Su, Chem. Phys. Lett. **374**, 170 (2003)
21. P. Hu, L.J. Yu, A.H. Zuo, C.Y. Guo, F.L. Yuan, J. Phys. Chem. C. **113**, 900 (2009)
22. N. Han, Y.J. Tian, X.F. Wu, Y.F. Chen, Sens. Actuators B **138**, 228 (2009)
23. B.C. Wu, R.H. Yuan, X.Z. Fu, J. Solid State Chem. **182**, 560 (2009)
24. H.G. Yang, H.C. Zeng, J. Phys. Chem. B **108**, 3492 (2004)
25. K. Zakrzewska, Vacuum **74**, 335 (2004)
26. W. Zeng, T.M. Liu, Physica B **405**, 564 (2010)
27. M.H. Seo, M. Yuasa, T. Kida, J.S. Huh, K. Shimanoe, N. Yamazoe, Sens. Actuators B **137**, 513 (2009)
28. A.M. More, J.L. Gunjakar, C.D. Lokhande, Sens. Actuators B **129**, 671 (2008)
29. S. Pokhrel, L.H. Huo, H. Zhao, S. Gao, Sens. Actuators B **129**, 18 (2008)